

Double cycle-consistent generative adversarial network for unsupervised conditional generation

Fei Ding, Feng Luo, Yin Yang
School of Computing, Clemson University
{feid, luofeng, yin5}@clemson.edu

Abstract

Conditional generative models have achieved considerable success in the past few years, but usually require a lot of labeled data. Recently, ClusterGAN combines GAN with an encoder to achieve remarkable clustering performance via unsupervised conditional generation. However, it ignores the real conditional distribution of data, which leads to generating less diverse samples for each class and makes the encoder only achieve sub-optimal clustering performance. Here, we propose a new unsupervised conditional generation framework, Double Cycle-Consistent Conditional GAN (DC3-GAN), which can generate diverse class-conditioned samples. We enforce the encoder and the generator of GAN to form an encoder-generator pair in addition to the generator-encoder pair, which enables us to avoid the low-diversity generation and the triviality of latent features. We train the encoder-generator pair using real data, which can indirectly estimate the real conditional distribution. Meanwhile, this framework enforces the outputs of the encoder to match the inputs of GAN and the prior noise distribution, which disentangles latent space into two parts: one-hot discrete and continuous latent variables. The former can be directly expressed as clusters and the latter represents remaining unspecified factors. This work demonstrates that enhancing the diversity of unsupervised conditional generated samples can improve the clustering performance. Experiments on different benchmark datasets show that the proposed method outperforms existing generative model-based clustering methods, and also achieves the optimal disentanglement performance.

1. Introduction

Generative Adversarial Networks (GANs) have achieved remarkable success in realistic image generation such as class-conditioned generation [22, 21], but at the cost of collecting massive amounts of annotated images. Given a large number of unlabeled images available online, how to lever-

age them for conditional generation remains a challenging problem. As an important unsupervised learning method, clustering has been widely used in many computer vision applications, such as image segmentation [8], visual features learning [4], and 3D object recognition [46]. Therefore, it's natural to combine clustering and generative models for an unsupervised conditional generation.

When processing high-semantic and high-dimensional images, most clustering methods such as DEC [51], DCN [52], and ClusterGAN [37], have been proposed to learn the 'clustering-friendly' latent representations, then perform clustering algorithms, such as K-means [31] on the latent space. Since there are multiple optimization objectives, such as adversarial training for generation, low-dimensional representation learning, and distance-based clustering algorithms for class assignments, it's optimal to effectively integrate them to achieve unsupervised conditional generation in an end-to-end manner. Recently, the ClusterGAN [37] provides a new clustering mechanism based on the GAN and the inverse-mapping network. However, it only focuses on learning non-smooth latent space for clustering, and ignores the estimation of the real conditional distribution, leading to sub-optimal conditional generation.

In this paper, we introduce a novel unsupervised conditional generative model called Double Cycle-Consistent Conditional GAN (DC3-GAN). It can generate diverse samples for each class without labels, and then directly obtains clusters without additional clustering methods. This framework can accommodate conditional generation and clustering in a unified and end-to-end manner. Moreover, we introduce a solution for directly obtaining class assignment by disentangling the latent space into two parts: the one-hot discrete latent variables directly related to categorical cluster information, and the continuous latent variables related to other factors of variations. The disentanglement of latent space is performing the clustering operation. Unlike the existing distance-based clustering methods, our method does not need any explicit clustering objectives or distance/similarity calculations in the latent space.

The conditional generation usually requires labels to es-

timate the real conditional distribution. But this work focuses on the unsupervised conditional generation, hence we propose to indirectly estimate the real conditional distribution via two cycle-consistencies: the generator-encoder pair and the encoder-generator pair. We first construct the generator-encoder pair with the generator of GAN and the encoder, which involves the mapping from latent space to data space, and back to latent space, to separate the latent space into one-hot discrete variables and continuous variables of other factors. Then, we utilize a weight sharing strategy to form a deterministic encoder-generator pair under the maximum mean discrepancy (MMD) regularization [14]. Our method can be considered as the integration of the GAN and deterministic Autoencoder to achieve the unsupervised conditional generation. A better generator helps to guide the encoder for training, and a better encoder in turn helps to generate better class-conditioned samples. Therefore, we apply clustering as a proxy task to evaluate the estimation of the real conditional distribution. This framework includes three different types of regularizations: an adversarial density-ratio loss in data space, MMD loss in the continuous latent code, and cross-entropy loss in discrete latent code. The source code and models are publicly available at this link ¹.

In summary, our contributions are as follows:

(1) We propose a new unsupervised conditional GAN framework called DC3-GAN, which can achieve effective conditional generation without labels, and directly obtain cluster assignments without clustering methods.

(2) We combine the encoder-generator pair with the generator-encoder pair to form two cycle-consistencies, which help avoid the triviality on continuous latent variable and enables estimation of the real conditional distribution.

(3) We evaluate the conditional generation quality of DC3-GAN, and apply it to different benchmark datasets for disentanglement and clustering. The experiments demonstrate that it can achieve desirable disentanglement and clustering performance in most cases.

2. Method

Given a collection i.i.d. samples $\mathbf{x} = \{x^i\}_{i=1}^N$ (e.g., images) drawn from an unknown data distribution P_x , where x^i is the i -th data sample and N is the size of the dataset, the standard GAN [13, 15] consists of two components: the generator G_θ and the discriminator D_ψ . G_θ defines a mapping from the latent space \mathcal{Z} to the data space \mathcal{X} and D_ψ can be considered as a mapping from the data space \mathcal{X} to the probability of one sample being real or not. To achieve unsupervised conditional generation, we need to introduce an inference network E_ϕ to obtain the latent variables given the data sample.

In this section, we first conduct a comprehensive analysis of ClusterGAN [37], and observe that there is a key loss item missing in the objective. To address this issue, we introduce an MMD-based regularization to enforce the inference network and the generator of standard GAN to form a deterministic Autoencoder. Meanwhile, the method enables us to disentangle the latent space \mathbf{z} into the one-hot discrete latent variables \mathbf{z}_c , and the continuous latent variables \mathbf{z}_n in an unsupervised manner. \mathbf{z}_c naturally represents the categorical cluster information; \mathbf{z}_n is expected to contain information of other variations.

2.1. Unsupervised conditional generation

ClusterGAN [37] provides a new clustering method using GANs, which utilizes a joint distribution of discrete and continuous latent variables as the prior of GANs. Although it focuses on projecting the data to the latent space for clustering, it can be generalized to an unsupervised conditional generation framework. And the optimization is based on the combination of original GAN loss, cycle-consistency loss, and cross-entropy loss.

$$\begin{aligned} \min_{G,E} \max_D \mathcal{L}_{\text{Clus}}(G, D, E) = & \underbrace{\mathbb{E}_{\mathbf{x} \sim P_x} [q(D_\psi(\mathbf{x}))]}_{\textcircled{1}} + \underbrace{\mathbb{E}_{\mathbf{z}_c \sim P_c, \mathbf{z}_n \sim P_n} [q(1 - D_\psi(G_\theta(\mathbf{z}_c, \mathbf{z}_n)))]}_{\textcircled{2}} \\ & - \lambda_n \underbrace{\mathbb{E}_{\mathbf{z}_c \sim P_c, \mathbf{z}_n \sim P_n} [c(E_\phi(G_\theta(\mathbf{z}_c, \mathbf{z}_n))_n, \mathbf{z}_n)]}_{\textcircled{2}} \\ & - \lambda_c \underbrace{\mathbb{E}_{\mathbf{z}_c \sim P_c, \mathbf{z}_n \sim P_n} [c(E_\phi(G_\theta(\mathbf{z}_c, \mathbf{z}_n))_c, \mathbf{z}_c)]}_{\textcircled{3}}, \end{aligned} \quad (1)$$

where P_x is the real data distribution, P_c is the prior distribution of \mathbf{z}_c , and P_n is the prior distribution of \mathbf{z}_n . $c(\cdot, \cdot)$ is any measurable cost function, λ_n and λ_c are hyperparameters balancing these losses. For the original GAN [13], the function q is chosen as $q(t) = \log t$, and the Wasserstein GAN [15] applies $q(t) = t$. This adversarial density-ratio estimation [45] enforces Q_x to match P_x , as shown in term $\textcircled{1}$, \mathcal{L}_{GAN} . The term $\textcircled{2}$ and $\textcircled{3}$ are two constraints to the generator G_θ and the encoder E_ϕ , which correspond to the cycle-consistency of \mathbf{z}_n and the cross-entropy loss on \mathbf{z}_c .

To analyze this clearly, the term $\textcircled{2}$ can be written as:

$$\begin{aligned} \mathcal{L}_n(G, E) = & -\mathbb{E}_{(\mathbf{x}, \mathbf{z}_n) \sim Q_{x,c}} [c(E_\phi(\mathbf{x})_n, \mathbf{z}_n)] \\ = & \mathbb{E}_{\mathbf{z}_c \sim P_c, \mathbf{z}_n \sim P_n} [\|E_\phi(G_\theta(\mathbf{z}_c, \mathbf{z}_n)) - \mathbf{z}_n\|]. \end{aligned} \quad (2)$$

Thus, this loss term attempts to keep the cycle-consistency of \mathbf{z}_n during optimization. After adding the recovery of \mathbf{z}_n , the information from \mathbf{z}_n can be utilized for generation to a certain extent. However, since the dimension of \mathbf{x} is much larger than the dimensions of \mathbf{z}_c and \mathbf{z}_n , this constraint may

¹after the paper is accepted

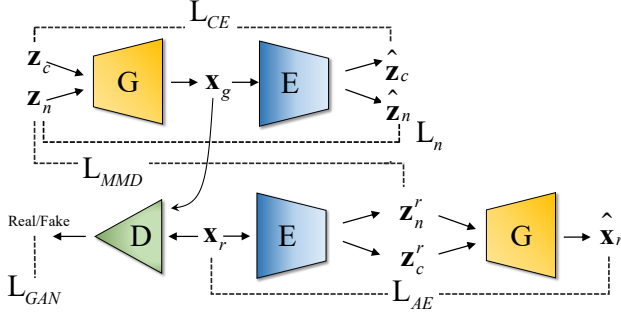


Figure 1. The architecture of DC3-GAN (G: generator, E: encoder, D: discriminator). The latent representations are separated into one-hot discrete latent variables \mathbf{z}_c and other factors of variation \mathbf{z}_n . The \mathbf{z}_c and \mathbf{z}_n are concatenated and fed into the G_θ for generation and the E_ϕ maps the samples (\mathbf{x}_g and \mathbf{x}_r) back into latent space. The D_ψ is adopted for the adversarial training in the data space. Note that all generators share the same parameters and all encoders share the same parameters.

become trivial for the generator-encoder (G-E) pair, and result in the generation of low-diversity samples.

The term ③ is the cross-entropy loss on \mathbf{z}_c :

$$\mathcal{L}_{CE}(G, E) = -\mathbb{E}_{(\mathbf{x}, \mathbf{z}_c) \sim Q_{\mathbf{z}_c}} [\log(Q^E(\mathbf{z}_c|\mathbf{x}))], \quad (3)$$

where $Q^E(\mathbf{z}_c|\mathbf{x})$ is used to denote the conditional distribution induced by E_ϕ . $Q_{\mathbf{z}_c|\mathbf{x}}$ is the conditional distribution specified by the generator G. Therefore, minimizing loss term $\mathcal{L}_{CE}(G, E)$ is equivalent to minimizing the KL divergence between $Q_{\mathbf{z}_c|\mathbf{x}}$ and $Q_{\mathbf{z}_c|\mathbf{x}}^E$. However, ClusterGAN ignores the real data conditional distributions $P_{\mathbf{z}_c|\mathbf{x}}$ in the objective, which usually requires real category information to estimate. Even when the marginal distributions P_x and Q_x match perfectly through the term ①, ClusterGAN still can not guarantee that two conditional distributions $P_{\mathbf{z}_c|\mathbf{x}}$ and $Q_{\mathbf{z}_c|\mathbf{x}}^E$ are well matched. Only minimizing $\mathcal{L}_{CE}(G, E)$ makes G tend to generate data that are far from the decision boundaries of E_ϕ . In other words, the generated images for each category may be easily distinguishable by E_ϕ , but have low intra-class diversity. It is thus essential to incorporate $P_{\mathbf{z}_c|\mathbf{x}}$ in the objective function.

2.2. The encoder-generator pair

Our above analysis of ClusterGAN reveals that simply adding an encoder cannot effectively achieve conditional generation, which has two main problems: trivial continuous latent variables recovery and missing real conditional distribution term, $P_{\mathbf{z}_c|\mathbf{x}}$. Therefore, we present to enforce E and G to form an Autoencoder (E-G pair) by introducing a distance-based regularizer. The real conditional distribution $P_{\mathbf{z}_c|\mathbf{x}}$ can also be estimated properly in an unsupervised

manner. We define the following objective:

$$\min_{G, E} \mathcal{L}_{E-G}(G, E) = \quad (4)$$

$$\mathbb{E}_{Q_\phi(\mathbf{z}_n, \mathbf{z}_c|\mathbf{x})} [\log P_\theta(\mathbf{x}|\mathbf{z}_n, \mathbf{z}_c)] + \lambda \cdot \mathcal{D}_z(Q_z, P_z),$$

where $\lambda > 0$ is a hyperparameter, \mathcal{D}_z is an arbitrary divergence between Q_z and P_z , which encourages the encoded distribution Q_z to match the prior P_z . Because the latent variables $\mathbf{z} = (\mathbf{z}_c, \mathbf{z}_n)$, and the prior distribution $P_z(\mathbf{z}_c, \mathbf{z}_n) = P_c(\mathbf{z}_c)P_n(\mathbf{z}_n)$, these constraints can be added by simply penalizing the discrete variables part and the continuous variables part separately.

The constraint of continuous variables \mathbf{z}_n can be considered to apply similar regularizations in the generative Autoencoder model like AAE [32] and WAE [44]. The former uses the GAN-based density-ratio trick to estimate the KL-divergence of distributions [45], and the latter minimizes the distance between distributions based on Maximum Mean Discrepancy (MMD) [14, 27]. We choose adversarial density-ratio estimation for modeling the data space because it can handle complex distributions. MMD-based regularizer is stable for optimization and works well with multivariate normal distributions [45]. Therefore, we choose MMD to quantify the distance between the prior distribution $P_n(\mathbf{z}_n)$ and the posterior distribution $Q_n(\mathbf{z}_n|\mathbf{x})$. Compared with WAE, we only penalize the continuous latent variables \mathbf{z}_n , not the whole latent variable. The regularizer \mathcal{D}_z based on MMD is expressed as:

$$\mathcal{L}_{MMD}(E) = \frac{1}{N(N-1)} \sum_{\ell \neq j} k(z_n^\ell, z_n^j) + \frac{1}{N(N-1)} \sum_{\ell \neq j} k(\hat{z}_n^\ell, \hat{z}_n^j) - \frac{2}{N^2} \sum_{\ell, j} k(z_n^\ell, \hat{z}_n^j), \quad (5)$$

where $k(\cdot, \cdot)$ can be any positive definite kernel, $\{z_n^1, \dots, z_n^N\}$ are sampled from the prior distribution $P_n(\mathbf{z}_n)$, \hat{z}_n^i is sampled from the posterior distribution $Q_n(\mathbf{z}_n|\mathbf{x})$ and x^i is sampled from the real data samples for $i = 1, 2, \dots, N$.

The constraint of \mathbf{z}_c can't be applied explicitly without labels. Instead, we use a mean absolute error (MAE) criterion to estimate the encoding distribution $Q_\phi(\mathbf{z}|\mathbf{x})$ and the decoding distribution $P_\theta(\mathbf{x}|\mathbf{z})$, which are taken to be deterministic and can be replaced by E_ϕ and G_θ , respectively.

$$\mathcal{L}_{AE}(E, G) = \mathbb{E}_{\mathbf{x} \sim P_x} [|\mathbf{x} - G_\theta(E_\phi(\mathbf{x}))|]. \quad (6)$$

2.3. The generator-encoder pair

In addition to the encoder-generator pair, it also necessary to emphasize the generator-encoder pair for the disentanglement between discrete and continuous latent variables, as shown in Figure 1. Most of the existing methods [17, 56, 41] leverage labels to achieve the disentanglement of various factors. This work attempts to encourage

independence between $Q_n(\mathbf{z}_n|\mathbf{x})$ and $Q_c(\mathbf{z}_c|\mathbf{x})$ as much as possible without labels.

We sample the latent variables $\mathbf{z} = (\mathbf{z}_c, \mathbf{z}_n)$ from the discrete-continuous prior, through the generator-encoder pair, it should output the identical discrete and continuous latent variables $(\hat{\mathbf{z}}_c, \hat{\mathbf{z}}_n)$. It enforces the generator to take advantage of extra information from \mathbf{z}_c . Besides, the recovery of latent variables ensure that outputs of the encoder E_ϕ are conditionally independent. When E_ϕ maps the real data sample \mathbf{x} to latent representations \mathbf{z}_c^r and \mathbf{z}_n^r , which are expected to be conditionally independent. The cross-entropy loss (Eq. 3) between \mathbf{z}_c and $\hat{\mathbf{z}}_c$ can ensure that the latent variables $\hat{\mathbf{z}}_c$ only contain class-related information. Besides, to ensure that the latent variables $\hat{\mathbf{z}}_c$ or $\hat{\mathbf{z}}_n^r$ don't contain any class-related information, it is necessary to apply additional regularizers to penalize $\hat{\mathbf{z}}_n$ and $\hat{\mathbf{z}}_n^r$, which are related to the loss \mathcal{L}_n and \mathcal{L}_{MMD} .

2.4. Objective of DC3-GAN

The objective function of our approach is integrated into the following form:

$$\mathcal{L} = \mathcal{L}_{\text{GAN}} + \mathcal{L}_{\text{AE}} + \beta_1 \mathcal{L}_{\text{MMD}} + \beta_2 \mathcal{L}_n + \beta_3 \mathcal{L}_{\text{CE}}. \quad (7)$$

where the regularization coefficients β_1 to $\beta_3 \geq 0$, balancing the weights of different loss terms. Each term of Eq. 7 plays a different role for three components: generator G_θ , discriminator D_ψ , and encoder E_ϕ . Both \mathcal{L}_{GAN} and \mathcal{L}_{AE} are related to G_θ and E_ϕ , which constrain the whole latent variables. The \mathcal{L}_{GAN} term is also related to D_ψ , which focuses on distinguishing the true data samples from the fake samples generated by G_θ . \mathcal{L}_{MMD} and \mathcal{L}_n are related to continuous latent variables, and \mathcal{L}_{CE} and \mathcal{L}_c are related to discrete latent variables. All these loss terms are used to ensure that our algorithm disentangles the latent space generated from encoder into cluster information and remaining unspecified factors. The training procedure of DC3-GAN applies jointly updating the parameters of G_θ , D_ψ and E_ϕ , as described in Appendix. We empirically set $\beta_1 = \beta_2$ to enable a reasonable adjustment of the relative importance of continuous and discrete parts.

3. Experiments

In this section, we perform a variety of experiments to evaluate the effectiveness of our proposed method, including clusters assignment via \mathbf{z}_c and visualization studies of \mathbf{z}_n . We also conduct ablation experiments to understand the contribution of various loss terms.

Data sets. The clustering experiments are carried out on seven datasets: MNIST [25], Fashion-MNIST [50], YouTube-Face (YTF) [49], Pendigits [1], 10x_73k [55], COIL-100 [38], and CIFAR-10 [24]. The disentanglement evaluation is conducted on dsprites [35]. Both of the first

two datasets contain 70k images with 10 categories, and each sample is a 28×28 grayscale image. YTF contains 10k face images of size 55×55 , belonging to 41 categories. The Pendigits dataset contains a time series of (x, y) coordinates of hand-written digits. It has 10 categories and contains 10992 samples, and each sample is represented as a 16-dimensional vector. The 10x_73k dataset contains 73233 data samples of single-cell RNA-seq counts of 8 cell types, and the dimension of each sample is 720. The multi-view object image dataset COIL-100 has 100 clusters and contains 7200 images of size 128×128 .

Implementation Details. We implement different neural network structures for G_θ , D_ψ , and E_ϕ to handle different types of data. We provide details of models in the Appendix. For the prior distribution of our method, we randomly generate the discrete latent code \mathbf{z}_c , which is equal to one of the elementary one-hot encoded vectors in \mathbb{R}^K , then we sample the continuous latent code from $\mathbf{z}_n \sim \mathcal{N}(\mathbf{0}, \sigma^2 \mathbf{I}_{d_n})$, here $\sigma = 0.10$. The sampled latent code $\mathbf{z} = (\mathbf{z}_c, \mathbf{z}_n)$ is used as the input of G_θ to generate samples. The dimensions of \mathbf{z}_c and \mathbf{z}_n are shown in Table 9. We implement the MMD loss with RBF kernel [44] to penalize the posterior distribution $Q_\phi(\mathbf{z}_n|\mathbf{x})$. The improved GAN variant with a gradient penalty [15] is used in all experiments. To obtain the cluster assignment, we directly use the argmax over all softmax probabilities for different clusters. The following regularization parameters work well during all experiments: $\lambda = 10$, $\beta_1 = \beta_2 = 0.1$, $\beta_3 = 10$. We implement the models using the TensorFlow library and train them on one NVIDIA DGX-1 station.

3.1. Evaluation of generation quality

Table 1. Comparison of FID score to reveal the quality of generated samples from GAN methods (Lower is better).

Method	Ours	ClusterGAN	WGAN	InfoGAN
MNIST	0.15	0.81	0.88	1.88
Fashion	0.67	0.91	0.95	11.04

To demonstrate the quality and diversity of generated samples from DC3-GAN, we first calculate the Frchet Inception Distance (FID) [19] score of generated samples, as shown in Table 1. The FID scores on MNIST and Fashion are significantly lower than those of ClusterGAN. Our method shows that the estimation of real conditional distribution can improve the quality of generated samples. Then we randomly sample 200 pairs of generated images from one category to calculate structural similarity (SSIM) [48, 47] for diversity evaluation on MNIST data. This evaluation method for diversity has also been used in AC-GAN [40]. The SSIM scores range between 0.0 and 1.0, and lower mean scores indicate that samples from the same class are less similar. As shown in Table 2, our

Table 2. Comparison of mean SSIM scores of 200 pairs to reveal the diversity of generated samples from GAN methods (Lower is better).

Class	0	1	2	3	4	5	6	7	8	9
ClusterGAN	0.362	0.599	0.263	0.314	0.315	0.282	0.351	0.388	0.340	0.427
Ours	0.343	0.576	0.231	0.316	0.312	0.259	0.322	0.392	0.336	0.377

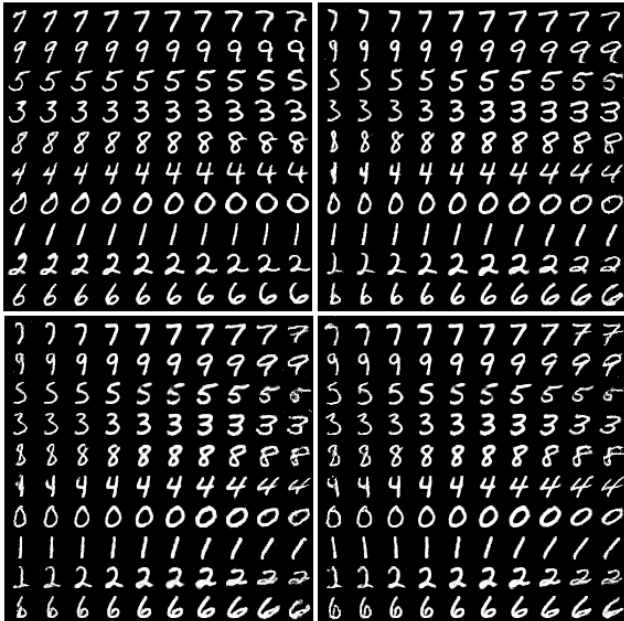


Figure 2. Samples generated on fixed discrete latent codes from the models trained on MNIST.

method achieves lower SSIM scores on most classes, which demonstrates that it can enhance the diversity of generation. The diversity of generated images indicates that there exist different latent variables for generative factors, except the cluster information. To further understand these generative factors, we change the value of one single dimension from $[-0.5, 0.5]$ in z_n while fixing other dimensions and the discrete latent variables z_c . As shown in Figure 2, the value changing leads to semantic changes in generated samples. The changed dimensions represent the tilt, style, and width factors of digits, which shows the potential to disentangle the latent space.

3.2. Evaluation of disentanglement

We further explore the disentanglement capability of DC3-GAN on dSprites dataset. We follow the same experimental settings and hyperparameters tuning as FactorVAE [23], InfoGAN [7] and InfoGAN-CR [28] for fair comparisons. We provide the experimental details in Appendix, and focus on explaining the results in this section. As shown in Table 3, our method also achieves excellent disentanglement performance. Compared with InfoGAN-

CR, we implement the proposed double-cycle consistency to replace the contrastive regularizer (CR) based on the InfoGAN architecture, which has two latent variables. These consistencies force the generator to generate different samples while fixing one latent variable and changing another latent variable. This is beneficial for disentanglement, as it simulates the latent traversal experiments and encourages distinct changes in generated samples. In addition, ModelCentrality is proposed by [28] for unsupervised model selection to evaluate the trained models on an unlabelled dataset. It's naturally suitable for our unsupervised conditional generation settings.

3.3. Evaluation of clustering algorithm

We argue that the clustering task can be considered as a proxy to evaluate the real conditional distribution estimation. To evaluate clustering results, we report two standard evaluation metrics: Clustering Purity (ACC) and Normalized Mutual Information (NMI). We compare DC3-GAN with four clustering baselines: K-means [31], Non-negative Matrix Factorization (NMF) [26]. We also compare our method with the state-of-the-art clustering approaches based on GAN and Autoencoder, respectively. For GAN-based approaches, ClusterGAN [37] is chosen as it achieves the superior clustering performance compared to other GAN models (*e.g.*, InfoGAN). For Autoencoder-based methods such as DEC [51], DCN [52] and DEPICT [10], Dual Autoencoder Network (DualAE) [54] are used for comparison. In addition, the deep spectral clustering (SpectralNet) [43] and joint unsupervised learning (JULE) [53] are also included in the comparison.

Table 4 reports the best clustering metrics of different models from 5 runs. Our method achieves significant performance improvement on Fashion-10, YTF, Pendigits, and 10x_73k datasets than other methods. Particularly, while all other methods perform worse than K-means on the 16-dimensional Pendigit dataset, our method significantly outperforms K-means in both ACC (0.847 vs. 0.793) and NMI (0.803 vs. 0.730). DC3-GAN achieves the best ACC result on YTF dataset while maintaining comparable NMI value. For MNIST dataset, DC3-GAN achieves close to the best performance on both ACC and NMI metrics. To further evaluate the performance of DC3-GAN on large numbers of clusters, we compare our clustering method with K-means on Coil-100 dataset using three standard evaluation metrics: ACC, NMI, and Adjusted Rand Index (ARI). As shown in Table 5, DC3-GAN achieves better performance

Table 3. Comparison results based on different disentanglement metrics on the dSprites dataset. The score 1.0 denotes a perfect disentanglement. All the baseline results are from [28]. The proposed DC3-GAN achieves desirable scores in most cases. The implementation of DC3-GAN is based on the source code of InfoGAN-CR, and MC (ModelCentrality) denotes an unsupervised model selection scheme [28].

Model	FactorVAE	DCI	SAP	Explicitness	Modularity	MIG	BetaVAE
VAE	0.63 ± 0.06	0.30 ± 0.10	-	-	-	0.10	-
β -TCVAE	0.62 ± 0.07	0.29 ± 0.10	-	-	-	0.45	-
HFVAE	0.63 ± 0.08	0.39 ± 0.16	-	-	-	-	-
β -VAE	0.63 ± 0.10	0.41 ± 0.11	0.55	-	-	0.21	-
FactorVAE	0.82	-	-	-	-	0.15	-
FactorVAE (1.0)	0.79 ± 0.01	0.67 ± 0.03	0.47 ± 0.03	0.78 ± 0.01	0.79 ± 0.01	0.27 ± 0.03	0.79 ± 0.02
FactorVAE (10.0)	0.83 ± 0.01	0.70 ± 0.02	0.57 ± 0.0	0.79 ± 0.0	0.79 ± 0.0	0.40 ± 0.01	0.83 ± 0.0
FactorVAE (40.0)	0.82 ± 0.01	0.74 ± 0.01	0.56 ± 0.0	0.79 ± 0.0	0.77 ± 0.01	0.43 ± 0.01	0.84 ± 0.01
FactorVAE + MC	0.84 ± 0.0	0.73 ± 0.01	0.58 ± 0.0	0.80 ± 0.0	0.82 ± 0.0	0.37 ± 0.0	0.86 ± 0.0
IB-GAN	0.80 ± 0.07	0.67 ± 0.07	-	-	-	-	-
InfoGAN	0.82 ± 0.01	0.60 ± 0.02	0.41 ± 0.02	0.82 ± 0.0	0.94 ± 0.01	0.22 ± 0.01	0.87 ± 0.01
InfoGAN-CR + MC	0.92 ± 0.0	0.77 ± 0.0	0.65 ± 0.0	0.87 ± 0.0	0.99 ± 0.0	0.45 ± 0.0	0.99 ± 0.0
Ours + MC	0.936 ± 0.0	0.790 ± 0.0	0.634 ± 0.0	0.862 ± 0.0	0.985 ± 0.0	0.378 ± 0.0	0.998 ± 0.0

Table 4. Comparison of clustering algorithms on five benchmark datasets. The results marked by (*) are from existing sklearn.cluster.KMeans package. The dash marks (-) mean that the source code is not available or that running released code is not practical, all other results are from [37] and [54]. SpecNet and ClusGAN mean SpectralNet and ClusterGAN.

Method	MNIST		Fashion-10		YTF		Pendigits		10x_73k	
	ACC	NMI								
K-means	0.532	0.500	0.474	0.512	0.601	0.776	0.793*	0.730*	0.623*	0.577*
NMF	0.560	0.450	0.500	0.510	-	-	0.670	0.580	0.710	0.690
DEC	0.863	0.834	0.518	0.546	0.371	0.446	-	-	-	-
DCN	0.830	0.810	-	-	-	-	0.720	0.690	-	-
JULE	0.964	0.913	0.563	0.608	0.684	0.848	-	-	-	-
DEPICT	0.965	0.917	0.392	0.392	0.621	0.802	-	-	-	-
SpecNet	0.800	0.814	-	-	0.685	0.798	-	-	-	-
InfoGAN	0.890	0.860	0.610	0.590	-	-	0.720	0.730	0.620	0.580
ClusGAN	0.950	0.890	0.630	0.640	-	-	0.770	0.730	0.810	0.730
DualAE	0.978	0.941	0.662	0.645	0.691	0.857	-	-	-	-
Ours	0.976	0.941	0.693	0.669	0.721	0.790	0.847	0.803	0.905	0.820

on all three metrics.

3.4. Evaluation on more images

We also use the t-SNE [30] algorithm to visualize z_n of MNIST datasets and compare them to ClusterGAN and the original data. As shown in Figure 3, we can observe different categories in the original data. In ClusterGAN, there are still several distinguishable clusters. In contrast, our method can make these points more cluttered in latent space, which doesn't contain obvious category information in the z_n . Therefore, our method demonstrates another excellent capability: all these informative continuous factors are independent of cluster information.

We first evaluate the scalability of DC3-GAN to large numbers of clusters on the COIL-100 dataset (100 clusters). Here, we compare our clustering method with K-means on three standard evaluation metrics: ACC, NMI and

Table 5. The clustering results on the Coil-100 dataset, which has a large number of clusters (K=100).

Method	ACC	NMI	ARI
K-means	0.668	0.836	0.574
ClusterGAN	0.615	0.797	0.487
Our method	0.822	0.911	0.764

Adjusted Rand Index (ARI). As shown in Table 5, DC3-GAN achieves better performance on all three metrics. DC3-GAN even gains an increase of 0.154 on ACC metric. We also perform image generation task on Coil-100 dataset, to further verify the generative performance, which involves mapping latent variables to the data space. Figure 4 shows the generated samples by fixing one-hot discrete latent variables, which are diverse and realistic. The continuous latent variables represent meaningful factors such as the pose, location and orientation information of objects. Therefore,

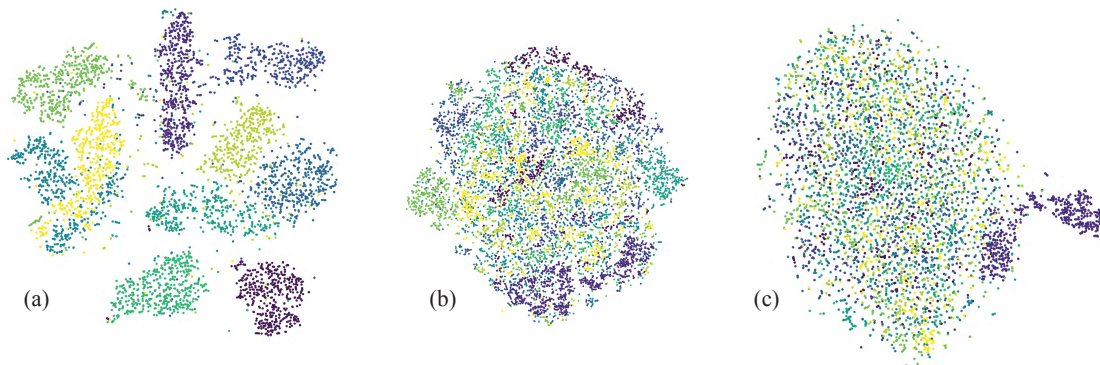


Figure 3. The t-SNE visualization of raw data (a), \mathbf{z}_n of ClusterGAN (b) and DC3-GAN (c) on MNIST dataset. The bulk of samples in the right part of a(3) is a small group of “1” images. The reason that they are not well mixed may be due to their low complexity.



Figure 4. The samples generated on fixed discrete latent variables from the models trained on Coil-100 dataset. Each column corresponds to a specific cluster.

the disentanglement of latent space not only provides the superior clustering performance, but also retains the remarkable ability of diverse and high-quality image generation.

Besides, we further evaluate the proposed method on more complex dataset: CIFAR-10. The implementation is based on Google compare-gan framework². The spectral normalization is used on both generator and discriminator. We use the same class-conditional BatchNorm in the generator as Lucic *et al.* [29], to incorporate the category information from \mathbf{z}_n . For the encoder, we use the pre-trained SimCLR [6] model to improving training efficiency, and apply 2-layer MLP as project head to map the learned representations to \mathbf{z}_n and \mathbf{z}_c . The self-supervised SimCLR model is pre-trained by following the official implementation³. Table 6 shows that DC3-GAN achieves close to the best clustering performance on ACC. Because our

²https://github.com/google/compare_gan

³<https://github.com/google-research/simclr>

method learns cluster memberships from conditional generation without labels, it’s also necessary to evaluate the generation results of images. As shown in Table 7, our method also maintains the quality of image generation, which enables to achieve the superior clustering results.

Table 6. CIFAR-10 images clustering results. All baseline results are from [20]. The value marked by (*) is the best (mean) results in [20], and they also report that avg. \pm STD is 0.576 ± 0.050 .

Method	ACC	NMI
K-means	0.229	0.087
DCGAN (2015) [42]	0.315	0.265
JULE (2016) [53]	0.272	0.192
DEC (2016) [51]	0.301	0.257
DAC (2017) [5]	0.522	0.396
DeepCluster (2018) [4]	0.374	-
ADC (2018) [18]	0.325	-
IIC (2019) [20]	0.617 (0.576)*	0.513
GATCluster(2020) [39]	0.610	0.475
Ours	0.605	0.484

3.5. Ablative Analysis

We perform the ablative analysis of our losses (Table 8). The \mathcal{L}_{AE} and \mathcal{L}_{MMD} are critical in our model. The inference network and the generator form a deterministic encoder-decoder pair. To minimize the reconstruction loss \mathcal{L}_{AE} , the generator G_θ needs to learn to generate realistic and diverse data samples. It also indirectly forces the \mathbf{z}_c^r

Table 7. FID results on the CIFAR-10 dataset (smaller is better). The results marked by (*) are from [33].

Method	FID Score
DCGANs [42]	29.7*
WGAN-GP (2017) [15]	29.3
SN-SMMDGAN (2018) [2]	25.0
MSGAN (2019) [33]	28.7*
Ours	28.5 \pm 0.02

Table 8. Ablations on MNIST dataset. Each row shows the removal of a loss term. The full setting includes all loss terms.

Ablative analysis	ACC	NMI
No \mathcal{L}_{CE}	0.899	0.863
No \mathcal{L}_n	0.868	0.0.851
No \mathcal{L}_{MMD}	0.812	0.829
No \mathcal{L}_{AE}	0.672	0.488
Full setting	0.976	0.941

to contain only the category information. \mathcal{L}_{MMD} enforces the posterior distribution $Q_\phi(\mathbf{z}_n|\mathbf{x})$ to be close to the prior distribution $P(\mathbf{z}_n)$. The clustering performance gain is also from the loss terms \mathcal{L}_{CE} and \mathcal{L}_n .

4. Related works

Latent space clustering. A general method to avoid the curse of dimensionality in clustering is mapping data samples to in a low-dimensional latent space and performing clustering on latent space. Most existing latent space clustering methods are based on Autoencoder [51, 9, 16, 52, 54], which enables reconstructing data samples from the low-dimensional representation. The training objectives usually are coupled with reconstruction loss to avoid random discriminative representations. However, it forces latent representations to capture all key factors of variations and similarities related to reconstruction, not class decision boundaries. Alternatively, recent contrastive learning utilizes instance discrimination to achieve remarkable self-supervised representation learning [6]. But it still has potential limitations that instance-level pseudo labels are from hand-crafted augmentations and cannot explicitly determine the underlying class boundaries. Such strategies may benefit from the good parameter initialization, but there is still a lack of stable supervision signals to directly improve class assignments. Furthermore, these latent space clustering methods still depend on additional distance-based clustering algorithms (*e.g.*, K-means) to obtain the cluster assignments. In contrast, our method accommodates the conditional generation and cluster assignments in an end-to-end manner.

Generative models. Learning disentangled representation can reveal the factors of variation in the data [3], and provides interpretable semantic latent codes for generative models. Generally, existing models can be mainly categorized into VAE-based and GAN-based types. The VAE-based methods involves extracting the label relevant and irrelevant representations [34, 17, 56, 41]. For example, Mathieu *et al.* [34] introduce a conditional VAE with adversarial training to disentangle the latent representations into label relevant and the remaining unspecified factors. Y-AE [41] focuses on the standard Autoencoder to achieve the disentanglement of implicit and explicit representations. Meanwhile, two-step disentanglement methods based on

Autoencoder [17] or VAE [56] are also proposed. However, all of these methods need to leverage (partial) label information. Besides, VAE usually can not achieve high-quality generation in real-world scenarios [11]. Therefore, several studies begin to capture discrete and continuous factors of variation based on GAN. InfoGAN [7] reveals the disentanglement of latent code by maximizing the mutual information between the latent code and the generated data, but it is not specifically designed for clustering. ClusterGAN [37] integrated GAN with an encoder network for clustering by creating a non-smooth latent space. However, it ignores the real conditional distribution, which leads to generate trivial latent features and less diverse samples. Unlike conventional conditional GANs [36], our proposed method integrates the Autoencoder and GAN by constructing two cycle-consistencies, and separates the latent variables into two parts without any labels.

5. Conclusion

In this work, we present DC3-GAN, a new conditional generation framework that can generate diverse samples without labels and directly obtain the cluster assignments without clustering methods. Unlike most existing latent space clustering algorithms, our method does not build ‘clustering-friendly’ latent space explicitly and does not need extra clustering operation. Therefore, our method avoids the difficulty of integrating latent feature construction and clustering. Furthermore, our method does not disentangle class relevant features from class non-relevant features. The disentanglement in our method is targeted to extract ‘cluster information’ from data. Although our method does not depend on any explicit distance calculation in the latent space, the distance between data may be implicitly defined by the neural networks.

The two cycle-consistencies ($\mathbf{x} \rightarrow (\mathbf{z}_c, \mathbf{z}_n) \rightarrow \mathbf{x}$, $(\mathbf{z}_c, \mathbf{z}_n) \rightarrow \mathbf{x} \rightarrow (\mathbf{z}_c, \mathbf{z}_n)$) in DC3-GAN can help avoid the triviality of \mathbf{z}_n , and then avoid the generation of low diversity images in some degree. We have used the real images to train the encoder-generation pair ($\mathbf{x} \rightarrow (\mathbf{z}_c, \mathbf{z}_n) \rightarrow \mathbf{x}$), which can help the encoder to estimate the real conditional distribution. However, due to the unsupervised fashion of clustering, the conditional distribution $Q(\mathbf{z}_c|\mathbf{x})$ specified by the generator of GAN may not match well with the true conditional distribution $P(\mathbf{z}_c|\mathbf{x})$ in real data, which is the case in both ClusterGAN and our DC3-GAN. This may be another reason for the low diversity conditional generation [12]. Improving GAN to create more diverse images is an important task for future work.

References

- [1] Fevzi Alimoglu and Ethem Alpaydin. Methods of combining multiple classifiers based on different representations for

- pen-based handwritten digit recognition. In *Proceedings of the Fifth Turkish Artificial Intelligence and Artificial Neural Networks Symposium (TAINN 96)*. Citeseer, 1996.
- [2] Michael Arbel, Dougal Sutherland, Mikołaj Bińkowski, and Arthur Gretton. On gradient regularizers for mmd gans. In *Advances in Neural Information Processing Systems*, pages 6700–6710, 2018.
 - [3] Yoshua Bengio, Aaron Courville, and Pascal Vincent. Representation learning: A review and new perspectives. *IEEE transactions on pattern analysis and machine intelligence*, 35(8):1798–1828, 2013.
 - [4] Mathilde Caron, Piotr Bojanowski, Armand Joulin, and Matthijs Douze. Deep clustering for unsupervised learning of visual features. In *Proceedings of the European Conference on Computer Vision (ECCV)*, pages 132–149, 2018.
 - [5] Jianlong Chang, Lingfeng Wang, Gaofeng Meng, Shiming Xiang, and Chunhong Pan. Deep adaptive image clustering. In *Proceedings of the IEEE International Conference on Computer Vision*, pages 5879–5887, 2017.
 - [6] Ting Chen, Simon Kornblith, Mohammad Norouzi, and Geoffrey Hinton. A simple framework for contrastive learning of visual representations. *arXiv preprint arXiv:2002.05709*, 2020.
 - [7] Xi Chen, Yan Duan, Rein Houthoofd, John Schulman, Ilya Sutskever, and Pieter Abbeel. Infogan: Interpretable representation learning by information maximizing generative adversarial nets. In *Advances in neural information processing systems*, pages 2172–2180, 2016.
 - [8] Keh-Shih Chuang, Hong-Long Tzeng, Sharon Chen, Jay Wu, and Tzong-Jer Chen. Fuzzy c-means clustering with spatial information for image segmentation. *computerized medical imaging and graphics*, 30(1):9–15, 2006.
 - [9] Nat Dilokthanakul, Pedro AM Mediano, Marta Garnelo, Matthew CH Lee, Hugh Salimbeni, Kai Arulkumaran, and Murray Shanahan. Deep unsupervised clustering with gaussian mixture variational autoencoders. *arXiv preprint arXiv:1611.02648*, 2016.
 - [10] Kamran Ghasedi Dizaji, Amirhossein Herandi, Cheng Deng, Weidong Cai, and Heng Huang. Deep clustering via joint convolutional autoencoder embedding and relative entropy minimization. In *Proceedings of the IEEE International Conference on Computer Vision*, pages 5736–5745, 2017.
 - [11] Partha Ghosh, Mehdi SM Sajjadi, Antonio Vergari, Michael Black, and Bernhard Schölkopf. From variational to deterministic autoencoders. *arXiv preprint arXiv:1903.12436*, 2019.
 - [12] Mingming Gong, Yanwu Xu, Chunyuan Li, Kun Zhang, and Kayhan Batmanghelich. Twin auxiliary classifiers gan. In *Advances in Neural Information Processing Systems*, pages 1328–1337, 2019.
 - [13] Ian Goodfellow, Jean Pouget-Abadie, Mehdi Mirza, Bing Xu, David Warde-Farley, Sherjil Ozair, Aaron Courville, and Yoshua Bengio. Generative adversarial nets. In *Advances in neural information processing systems*, pages 2672–2680, 2014.
 - [14] Arthur Gretton, Karsten M Borgwardt, Malte J Rasch, Bernhard Schölkopf, and Alexander Smola. A kernel two-sample test. *Journal of Machine Learning Research*, 13(Mar):723–773, 2012.
 - [15] Ishaan Gulrajani, Faruk Ahmed, Martin Arjovsky, Vincent Dumoulin, and Aaron C Courville. Improved training of wasserstein gans. In *Advances in neural information processing systems*, pages 5767–5777, 2017.
 - [16] Xifeng Guo, Long Gao, Xinwang Liu, and Jianping Yin. Improved deep embedded clustering with local structure preservation. In *IJCAI*, pages 1753–1759, 2017.
 - [17] Naama Hadad, Lior Wolf, and Moni Shahar. A two-step disentanglement method. In *Proceedings of the IEEE Conference on Computer Vision and Pattern Recognition*, pages 772–780, 2018.
 - [18] Philip Haeusser, Johannes Plapp, Vladimir Golkov, Elie Ajalbout, and Daniel Cremers. Associative deep clustering: Training a classification network with no labels. In *German Conference on Pattern Recognition*, pages 18–32. Springer, 2018.
 - [19] Martin Heusel, Hubert Ramsauer, Thomas Unterthiner, Bernhard Nessler, and Sepp Hochreiter. Gans trained by a two time-scale update rule converge to a local nash equilibrium. In *Advances in neural information processing systems*, pages 6626–6637, 2017.
 - [20] Xu Ji, João F Henriques, and Andrea Vedaldi. Invariant information clustering for unsupervised image classification and segmentation. In *Proceedings of the IEEE International Conference on Computer Vision*, pages 9865–9874, 2019.
 - [21] Tero Karras, Miika Aittala, Janne Hellsten, Samuli Laine, Jaakko Lehtinen, and Timo Aila. Training generative adversarial networks with limited data. In *Proc. NeurIPS*, 2020.
 - [22] Tero Karras, Samuli Laine, Miika Aittala, Janne Hellsten, Jaakko Lehtinen, and Timo Aila. Analyzing and improving the image quality of StyleGAN. In *Proc. CVPR*, 2020.
 - [23] Hyunjik Kim and Andriy Mnih. Disentangling by factorising. *arXiv preprint arXiv:1802.05983*, 2018.
 - [24] Alex Krizhevsky, Geoffrey Hinton, et al. Learning multiple layers of features from tiny images. 2009.
 - [25] Yann LeCun, Léon Bottou, Yoshua Bengio, Patrick Haffner, et al. Gradient-based learning applied to document recognition. *Proceedings of the IEEE*, 86(11):2278–2324, 1998.
 - [26] Daniel D Lee and H Sebastian Seung. Learning the parts of objects by non-negative matrix factorization. *Nature*, 401(6755):788, 1999.
 - [27] Yujia Li, Kevin Swersky, and Rich Zemel. Generative moment matching networks. In *International Conference on Machine Learning*, pages 1718–1727, 2015.
 - [28] Zinan Lin, Kiran Thekumparampil, Giulia Fanti, and Seungwoong Oh. Infogan-cr and modelcentrality: Self-supervised model training and selection for disentangling gans. In *International Conference on Machine Learning*, pages 6127–6139. PMLR, 2020.
 - [29] Mario Lucic, Michael Tschannen, Marvin Ritter, Xiaohua Zhai, Olivier Bachem, and Sylvain Gelly. High-fidelity image generation with fewer labels. *arXiv preprint arXiv:1903.02271*, 2019.
 - [30] Laurens van der Maaten and Geoffrey Hinton. Visualizing data using t-sne. *Journal of machine learning research*, 9(Nov):2579–2605, 2008.

- [31] James MacQueen et al. Some methods for classification and analysis of multivariate observations. In *Proceedings of the fifth Berkeley symposium on mathematical statistics and probability*, volume 1, pages 281–297. Oakland, CA, USA, 1967.
- [32] Alireza Makhzani, Jonathon Shlens, Navdeep Jaitly, Ian Goodfellow, and Brendan Frey. Adversarial autoencoders. *arXiv preprint arXiv:1511.05644*, 2015.
- [33] Qi Mao, Hsin-Ying Lee, Hung-Yu Tseng, Siwei Ma, and Ming-Hsuan Yang. Mode seeking generative adversarial networks for diverse image synthesis. In *Proceedings of the IEEE Conference on Computer Vision and Pattern Recognition*, pages 1429–1437, 2019.
- [34] Michael F Mathieu, Junbo Jake Zhao, Junbo Zhao, Aditya Ramesh, Pablo Sprechmann, and Yann LeCun. Disentangling factors of variation in deep representation using adversarial training. In *Advances in Neural Information Processing Systems*, pages 5040–5048, 2016.
- [35] Loic Matthey, Irina Higgins, Demis Hassabis, and Alexander Lerchner. dsprites: Disentanglement testing sprites dataset, 2017.
- [36] Mehdi Mirza and Simon Osindero. Conditional generative adversarial nets. *arXiv preprint arXiv:1411.1784*, 2014.
- [37] Sudipto Mukherjee, Himanshu Asnani, Eugene Lin, and Sreeram Kannan. Clustergan: Latent space clustering in generative adversarial networks. In *Proceedings of the AAAI Conference on Artificial Intelligence*, volume 33, pages 4610–4617, 2019.
- [38] Sameer A Nene, Shree K Nayar, Hiroshi Murase, et al. Columbia object image library (coil-20). 1996.
- [39] Chuang Niu, Jun Zhang, Ge Wang, and Jimin Liang. Gat-cluster: Self-supervised gaussian-attention network for image clustering. In *European Conference on Computer Vision*, pages 735–751. Springer, 2020.
- [40] Augustus Odena, Christopher Olah, and Jonathon Shlens. Conditional image synthesis with auxiliary classifier gans. In *International conference on machine learning*, pages 2642–2651. PMLR, 2017.
- [41] Massimiliano Patacchiola, Patrick Fox-Roberts, and Edward Rosten. Y-autoencoders: disentangling latent representations via sequential-encoding. *arXiv preprint arXiv:1907.10949*, 2019.
- [42] Alec Radford, Luke Metz, and Soumith Chintala. Unsupervised representation learning with deep convolutional generative adversarial networks. *arXiv preprint arXiv:1511.06434*, 2015.
- [43] Uri Shaham, Kelly Stanton, Henry Li, Boaz Nadler, Ronen Basri, and Yuval Kluger. Spectralnet: Spectral clustering using deep neural networks. *arXiv preprint arXiv:1801.01587*, 2018.
- [44] Ilya Tolstikhin, Olivier Bousquet, Sylvain Gelly, and Bernhard Schoelkopf. Wasserstein auto-encoders. *arXiv preprint arXiv:1711.01558*, 2017.
- [45] Michael Tschannen, Olivier Bachem, and Mario Lucic. Recent advances in autoencoder-based representation learning. *arXiv preprint arXiv:1812.05069*, 2018.
- [46] Chu Wang, Marcello Pelillo, and Kaleem Siddiqi. Dominant set clustering and pooling for multi-view 3d object recognition. *arXiv preprint arXiv:1906.01592*, 2019.
- [47] Zhou Wang and Alan C Bovik. Mean squared error: Love it or leave it? a new look at signal fidelity measures. *IEEE signal processing magazine*, 26(1):98–117, 2009.
- [48] Zhou Wang, Alan C Bovik, Hamid R Sheikh, and Eero P Simoncelli. Image quality assessment: from error visibility to structural similarity. *IEEE transactions on image processing*, 13(4):600–612, 2004.
- [49] Lior Wolf, Tal Hassner, and Itay Maoz. Face recognition in unconstrained videos with matched background similarity. In *Proceedings of the IEEE Conference on Computer Vision and Pattern Recognition*, pages 529–534, 2011.
- [50] Han Xiao, Kashif Rasul, and Roland Vollgraf. Fashion-mnist: a novel image dataset for benchmarking machine learning algorithms. *arXiv preprint arXiv:1708.07747*, 2017.
- [51] Junyuan Xie, Ross Girshick, and Ali Farhadi. Unsupervised deep embedding for clustering analysis. In *International conference on machine learning*, pages 478–487, 2016.
- [52] Bo Yang, Xiao Fu, Nicholas D Sidiropoulos, and Mingyi Hong. Towards k-means-friendly spaces: Simultaneous deep learning and clustering. In *Proceedings of the 34th International Conference on Machine Learning*, volume 70, pages 3861–3870. JMLR.org, 2017.
- [53] Jianwei Yang, Devi Parikh, and Dhruv Batra. Joint unsupervised learning of deep representations and image clusters. In *Proceedings of the IEEE Conference on Computer Vision and Pattern Recognition*, pages 5147–5156, 2016.
- [54] Xu Yang, Cheng Deng, Feng Zheng, Junchi Yan, and Wei Liu. Deep spectral clustering using dual autoencoder network. In *Proceedings of the IEEE Conference on Computer Vision and Pattern Recognition*, pages 4066–4075, 2019.
- [55] Grace XY Zheng, Jessica M Terry, Phillip Belgrader, Paul Ryvkin, Zachary W Bent, Ryan Wilson, Solongo B Ziraldo, Tobias D Wheeler, Geoff P McDermott, Junjie Zhu, et al. Massively parallel digital transcriptional profiling of single cells. *Nature communications*, 8:14049, 2017.
- [56] Zhilin Zheng and Li Sun. Disentangling latent space for vae by label relevant/irrelevant dimensions. In *Proceedings of the IEEE Conference on Computer Vision and Pattern Recognition*, pages 12192–12201, 2019.

A. Appendix

A.1. Training algorithm

Algorithm 1: The training procedure of DC3-GAN.

Input: θ, ψ, ϕ initial parameters of G_θ, D_ψ and E_ϕ , the dimension of latent code d_n , the number of clusters K , the batch size B , the number of critic iterations per end-to-end iteration M , the regularization parameters $\beta_1 - \beta_3$

Output: The parameters of G_θ, D_ψ and E_ϕ

Data: Training data set \mathbf{x}

```

1 while not converged do
2   for  $i=1, \dots, M$  do
3     Sample  $\mathbf{z}_n \sim P(\mathbf{z}_n)$  a batch of random noise
4     Sample  $\mathbf{z}_c$  a batch of random one-hot vectors
5      $\mathbf{z} \leftarrow (\mathbf{z}_c, \mathbf{z}_n)$ 
6      $\mathbf{x}_g \leftarrow G_\theta(\mathbf{z})$ 
7     Sample  $\mathbf{x}_r \sim P_x$  a batch of the training dataset
8      $\psi \leftarrow \nabla_\psi(D_\psi(\mathbf{x}_r) - D_\psi(\mathbf{x}_g))$ 
9     Sample  $\mathbf{z}_n \sim P(\mathbf{z}_n)$  a batch of random noise
10    Sample  $\mathbf{z}_c$  a batch of random one-hot vectors
11     $\mathbf{z} \leftarrow (\mathbf{z}_c, \mathbf{z}_n), \mathbf{x}_g \leftarrow G_\theta(\mathbf{z})$ 
12     $(\hat{\mathbf{z}}_c, \hat{\mathbf{z}}_n) \leftarrow E_\phi(\mathbf{x}_g)$ 
13     $(\mathbf{z}_c^r, \mathbf{z}_n^r) \leftarrow E_\phi(\mathbf{x}_r)$ 
14     $\mathbf{z}^r \leftarrow (\mathbf{z}_c^r, \mathbf{z}_n^r), \hat{\mathbf{x}}_r \leftarrow G_\theta(\mathbf{z}^r)$ 
15     $\theta \leftarrow \nabla_\theta(-D_\psi(G_\theta(\mathbf{z})) + |\mathbf{x}_r - \hat{\mathbf{x}}_r| + \beta_1 \text{MMD}(\mathbf{z}_n^r, \mathbf{z}_n) + \beta_2 \|\mathbf{z}_n - \hat{\mathbf{z}}_n\|_2^2 + \beta_3 \mathcal{H}(\mathbf{z}_c, \hat{\mathbf{z}}_c))$ 
16     $\phi \leftarrow \nabla_\phi(|\mathbf{x}_r - \hat{\mathbf{x}}_r| + \beta_1 \text{MMD}(\mathbf{z}_n^r, \mathbf{z}_n) + \beta_2 \|\mathbf{z}_n - \hat{\mathbf{z}}_n\|_2^2 + \beta_3 \mathcal{H}(\mathbf{z}_c, \hat{\mathbf{z}}_c))$ 

```

A.2. Implementation details

Table 9. The dimensions of \mathbf{z}_c and \mathbf{z}_n in DC3-GAN for different datasets. Note that the dimension of one-hot discrete latent variables \mathbf{z}_c is equal to the number of clusters.

Dataset	MNIST	Fashion-10	YTF	Pendigits	10x_73k	COIL-100	CIFAR-10
\mathbf{z}_c	10	10	41	10	8	100	10
\mathbf{z}_n	25	40	60	5	30	100	128

Table 10. The structure summary of the generator (G), discriminator (D), and encoder (E) in DC3-GAN for different datasets.

Dataset	Layer Type	G-1/D-4/E-4	G-2/D-3/E-3	G-3/D-2/E-2	G-4/D-1/E-1
MNIST	Conv-Deconv	$4 \times 4 \times 64$	$4 \times 4 \times 128$	-	-
Fashion-10	Conv-Deconv	$4 \times 4 \times 64$	$4 \times 4 \times 128$	-	-
YTF	Conv-Deconv	$5 \times 5 \times 32$	$5 \times 5 \times 64$	$5 \times 5 \times 128$	$5 \times 5 \times 256$
Pendigits	MLP	256	256	-	-
10x_73k	MLP	256	256	-	-

Table 9 summarizes the dimensions of latent variables for different datasets. And Table 10 summarizes the network structures for different datasets. For the image datasets (MNIST, Fashion-MNIST, and YTF), we employ the similar G_θ and D_ψ of DCGAN [42] with conv-deconv layers, batch normalization and leaky ReLU activations with a slope of 0.2. The E_ϕ uses the same architecture as D_ψ except for the last layer. For the Pendigits and 10x_73k datasets, the G_θ, D_ψ , and E_ϕ are the MLP with 2 hidden layers of 256 hidden units each. The model parameters have been initialized following the random normal distribution.

We evaluate our method on dSprites for disentanglement using the architectures shown in Table 11. The generator’s Adam learning rate is set to 0.001 and The learning rates of discriminator and encoder are set to 0.002. The total number of epoches is 28.

Table 11. The network structure of the generator (G), discriminator (D), and encoder (E) for dSprites experiments from [23]. We set the dimensions of continuous and noise variables to 5 as infoGAN-CR [28].

Discriminator D / Encoder E	Generator G
Input 64×64 binary image	Input $\in \mathbb{R}^{10}$
4×4 conv. 32 lReLU. stride 2	FC. 128 ReLU. batchnorm
4×4 conv. 32 lReLU. stride 2. batchnorm	FC. $4 \times 4 \times 64$ ReLU. batchnorm
4×4 conv. 64 lReLU. stride 2. batchnorm	4×4 upconv. 64 lReLU. stride 2. batchnorm
4×4 conv. 64 lReLU. stride 2. batchnorm	4×4 upconv. 32 lReLU. stride 2. batchnorm
FC. 128 lReLU. batchnorm (*)	4×4 upconv. 32 lReLU. stride 2. batchnorm
From *: FC. 1 sigmoid. (output layer for D)	4×4 upconv. 1 sigmoid. stride 2
From *: FC. 128 lReLU. batchnorm. FC 10 for E	

Table 12. The network structure for CIFAR-10 dataset from https://github.com/google/compare_gan. The ResBlock is the resample of the residual block with downsampling and upsampling. The input shape of images is $32 \times 32 \times 3$. The kernel size is described in the format $[filter_h, filter_w, stride]$ and the output shape is described as $h \times w \times channels$.

Discriminator D			Generator G		
LAYER	KERNEL	OUTPUT	LAYER	KERNEL	OUTPUT
ResBlock	[3,3,1]	$16 \times 16 \times 128$	z	-	128
ResBlock	[3,3,1]	$8 \times 8 \times 128$	Linear	-	$4 \times 4 \times 256$
ResBlock	[3,3,1]	$8 \times 8 \times 128$	ResBlock	[3,3,1]	$8 \times 8 \times 256$
ResBlock	[3,3,1]	$8 \times 8 \times 128$	ResBlock	[3,3,1]	$16 \times 16 \times 256$
ReLU, Mean Pooling	-	128	ResBlock	[3,3,1]	$32 \times 32 \times 256$
Linear	-	1	BN, ReLU	-	$32 \times 32 \times 256$
			Conv, Sigmoid	[3,3,1]	$32 \times 32 \times 3$

We also evaluate our method on CIFAR-10 dataset in a fully unsupervised settings. The architectures are shown in Table 12. We use the Adam optimizer with a learning rate 0.0002 for the generator, the discriminator and the encoder ($\beta_1 = 0.5, \beta_2 = 0.999$). We train the model with 5 discriminator steps before each generator and encoder step. The dimension of \mathbf{z}_n is fixed to 128, and the batch size is set to 64. The spectral normalization is used on both generator and discriminator. We use the same class-conditional BatchNorm in the generator as Lucic *et al.* [29], to incorporate the category information from \mathbf{z}_n . For the encoder, we combine the pre-trained SimCLR [6] model and trainable 2-layer MLP with hidden size 512 and output size 138 (dimensions of \mathbf{z}_n and \mathbf{z}_c). The self-supervised SimCLR model is pre-trained by following the official implementation ⁴. The reasons of choosing pre-trained SimCLR model are based on reducing the parameters of encoder, and improving training efficiency. Different from previous experiments, we apply the following regularization parameters on CIFAR-10 dataset: $\beta_1 = \beta_2 = 1, \beta_3 = 1$.

⁴<https://github.com/google-research/simclr>